CST014

Prediction of Boundary Layer Flow Transition under Non-Zero Pressure Gradient Conditions using Boundary-Fitted Technique

K. Suluksna[1*], V. Juntasaro[2], and E. Juntasaro[1]

[1] School of Mechanical Engineering, Institute of Engineering, Suranaree University of Technology,
Nakhon Ratchasima 30000, Thailand,
Tel: 0-4422-4410-1, Fax: 0-4422-4613, *E-mail: keerati@sut.ac.th
[2] Department of Mechanical Engineering, Faculty of Engineering, Kasetsart University,
Bangkhen, Bangkok 10900, Thailand,
Tel: 0-2942-8555 ext 1829, Fax: 0-2579-4576, E-mail: fengvrj@ku.ac.th

Abstract

A numerical technique to investigate the transitional boundary layer flow over a flat plate subjected to freestream turbulence and non-zero pressure gradient is presented. The technique solves the full equations of fluid motion rather than the boundary-layer equations which are neglect the y-momentum equation and preserve the pressure variation only along the streamwise direction. In the present technique, the y-momentum equation remains employed to maintain the full-step computation and furthermore the pressure is treated as the flow variable and the effect of the pressure variation along the streamwise direction is deliberately converted to the variation of domain thickness along the same direction according to the test section of Coupland (1993), for T3C1, T3C2 and T3C4 cases. The boundary-fitted technique to transform the nonuniform grids to the uniform rectangular grids is used. The performance of two well-known turbulence models: the k-ε model of Launder and Sharma (1974) and the SST turbulence model of Menter (1994), in predicting the transitional boundary layer is assessed against the experimental data.

Keywords: Transition, Non-zero pressure gradient, Freestream turbulence intensity, Boundary layer

1. Introduction

Flow transition plays an important role in the design and performance of turbomachinery applications and aerospace devices where the wall-shear-stress or wall-heat-transfer or a combination of both is of interest. The boundary layer flows in turbomachines usually involve flow transition under the effects of several factors, such as freestream turbulence, pressure gradient, heat transfer, etc. [1]. In turbomachinery, the flow in the cascade passages can result in the boundary layer of the blade being transitional over 20-70% of the blade surface. The change in any properties related to the transition can therefore have a strong influence on the operation and hence the performance [2]. As a result, the performance, weight and cost associated with turbomachines can be affected by transition and the prediction of its behavior is an important element in analysis and performance evaluation and ultimately in the design of more efficient system [3].

The transitional boundary layer flow over a flat plate subjected to freestream turbulence serves as a simple valuable tool in testing the performance of the turbulence models in predicting the transition behaviour. Interestingly, in the past, typical testing has been demonstrated on either the boundary layer flow with zero-pressure gradient or on complex geometry applications such as airfoil, aerospace devices, turbine blade, etc., in which case can directly employ the full equations of fluid motion: the continuity and momentum equations, without any modification to such equations. This is because the computational domain, together with the boundary conditions, for the boundary layer flow with zero-pressure gradient can easily be setup by which the computational domain can be constructed with the same thickness throughout in rectangular shape, and the pressure condition for all boundaries is the zero normal gradients. Unlike the case of the boundary layer with non-zero pressure gradient where the flow has been concerned with the pressure variation and, in the present work, such variation along the flow direction is known in advance from the experimental data. As a result, based on the idea of Prandtl (1904) by performing on the order-of-magnitude assumptions, the three full equations of fluid motion, in case of two-dimensional flow analysis, will be reduced to Prandtl's two boundary layer equations as follows:

$$\frac{\partial \rho uu}{\partial x} + \frac{\partial \rho vu}{\partial y} \approx \rho U \frac{dU}{dx} + \frac{\partial \tau}{\partial y}, \tag{1}$$

$$\frac{\partial \rho u}{\partial x} + \frac{\partial \rho v}{\partial y} = 0. \tag{2}$$

It is clear that the features of such boundary-layer equations are quite different from the full equations of fluid motion in which the y-momentum equation is

School of Mechanical Engineering , Suranaree University of Technology

CST014

---

neglected due to a very small magnitude of the v velocity compared with the u velocity and the pressure is also assumed to be varied only along the streamwise direction which is known in advance from Bernoulli's equation applied to the outer inviscid flow. As a result, the full-step computation cannot be performed on the boundary-layer equations because the number of the equations in the boundary-layer equations is not sufficient to be solved. However, deciding to perform the calculation with the full equations of fluid motion to maintain the full-step computation may not take into account the pressure gradient variation, which is exactly known in advance, in the momentum equations directly. This is because if the pressure field is correctly known, the resulting velocity will satisfy the continuity and the pressure correction which is used to correct the pressure and velocity fields in the SIMPLE algorithm is not vital. Unfortunately, this concept is actually incorrect because the pressure correction is directly related to the continuity which is always a vital part of any fluid-flow analysis.

In the present study, the full equations of fluid motion are investigated rather than the simplified form of the boundary-layer equations. The y-momentum equation is also preserved in the computation algorithm and the pressure is treated as the flow variable rather than imposed as the source term in the momentum equations even though its variation is known in advance form the experimental data. The effect of the pressure variation along the streamwise direction has been converted to the variation of domain thickness along the same direction. The performance of two popular turbulence models: the k-ε model of Launder and Sharma [4] and the SST turbulence model of Menter [5], in predicting the transition are assessed in comparison with the experimental data of Coupland [6] in cases of T3C1, T3C2, and T3C4.

2. Turbulence Models

The turbulence models investigated in the present study are the k-ε model of Launder and Sharma [4] and the SST model of Menter [5]. The transport equations of both models and the eddy viscosity models are written below.

2.1 The k-ε Model of Launder and Sharma (1974)

The low-Reynolds-number k-ε model of Launder and Sharma [4] is the most widely used. The model is very sophisticated and consists of two transport equations, which must be solved: one for the turbulent kinetic energy, k, and the other for the rate of dissipation of turbulent kinetic energy, ε. This model is generally derived from high-Reynolds-number model by introducing damping functions to account for the effect of the wall on turbulence. The assumption of this model is based on the Boussinesq hypothesis in which the turbulent stress is linearly related to the mean rate of strain as in a laminar flow, that is, the turbulent viscosity is presumed to be isotropic (the same in all directions). Unfortunately, this assumption fails in many categories of flow such as flows with boundary layer separation and

reattachment, secondary flow in duct and in turbomachinery, etc., where it leads to inaccurate flow prediction. A well-known shortcoming of this model stems largely from the turbulence being represented by its kinetic energy, which is scalar, and that the turbulent kinetic energy k is not the appropriate velocity scale close to solid boundaries. The transport equations for the kinetic energy and the dissipation rate of turbulence for this model are as follows:

$$\frac{\partial \rho u_j k}{\partial x_j} = \frac{\partial}{\partial x_j}\left[\left(\mu + \frac{\mu_t}{\sigma_k}\right)\frac{\partial k}{\partial x_j}\right] + P_k - \rho(\tilde{\varepsilon} + \varepsilon_w), \quad (3)$$

$$\frac{\partial \rho u_j \tilde{\varepsilon}}{\partial x_j} = \frac{\partial}{\partial x_j}\left[\left(\mu + \frac{\mu_t}{\sigma_\varepsilon}\right)\frac{\partial \tilde{\varepsilon}}{\partial x_j}\right] + C_{\varepsilon 1} f_{\varepsilon 1} \frac{\tilde{\varepsilon}}{k} P_k$$
$$- \rho C_{\varepsilon 2} f_{\varepsilon 1} \frac{\tilde{\varepsilon}^2}{k} + \phi_\varepsilon \quad (4)$$

The eddy viscosity is obtained from

$$\mu_t = \rho C_\mu f_\mu k^2 / \tilde{\varepsilon}. \quad (5)$$

The explicit wall terms are given by

$$\varepsilon_w = 2\mu_t \frac{\mu}{\rho}\left(\frac{\partial^2 u_i}{\partial x_j \partial x_k}\right)^2 \text{ and } \phi_\varepsilon = \frac{2\mu}{\rho}\left(\frac{\partial \sqrt{k}}{\partial x_j}\right)^2. \quad (6)$$

The model constants and damping functions are as follows:

$$C_\mu = 0.09, \ C_{\varepsilon 1} = 1.44, \ C_{\varepsilon 2} = 1.92, \quad (7)$$

$$\sigma_k = 1.0, \ \sigma_\varepsilon = 1.3, \quad (8)$$

$$f_\mu = \exp\left[-3.4(1 + 0.02 \, \text{Re}_t)^{-2}\right], \quad (9)$$

$$f_{\varepsilon 1} = 1, \ f_{\varepsilon 2} = 1 - 0.3\exp(\text{Re}_t^2), \quad (10)$$

where $\text{Re}_t = \rho k^2/(\mu\tilde{\varepsilon})$ is the turbulent Reynolds number.

The boundary conditions for the turbulence kinetic energy and its dissipation rate at solid wall are $k=0$ and $\tilde{\varepsilon}=0$.

2.2 The SST Model of Menter (1994)

The k-ω Shear Stress Transport (SST) turbulence model of Menter [5] merges the k-ω model of Wilcox with a high-Reynolds-number k-ε model (transformed into the k-ω formulation). The SST model seeks to combine the positive features of both models. Therefore, the k-ω approach is employed in the viscous sublayer of the boundary layer. The reason is that the k-ω model needs no damping function. This leads, for the same degree of accuracy, to the significantly higher numerical stability in comparison to the k-ε model. Furthermore, the k-ω model is also utilized in the logarithmic part of the boundary layer, where it is superior to the k-ε approach in adverse pressure gradient flows and compressible flows. On the other hand, the k-ε model is strongly sensitive to

School of Mechanical Engineering , Suranaree University of Technology

the freestream value of ω. The k-ε is also used in free-shear layers since it represents a fair compromise in accuracy for wakes, jets, and mixing layers. The disadvantage of the SST model is that distances to the nearest wall have to be known explicitly. This requires special provisions on multiblock structure or on unstructured grids. The transport equations for the kinetic energy and its specific dissipation rate of turbulence for the SST model are as follows:

$$\frac{\partial \rho u_j k}{\partial x_j} = \rho P_k - \rho \alpha^* \omega k + \frac{\partial}{\partial x_j}\left[(\mu + \sigma_k \mu_t)\frac{\partial k}{\partial x_j}\right], \qquad (11)$$

$$\frac{\partial \rho u_j \omega}{\partial x_j} = \frac{\partial}{\partial x_j}\left[(\mu + \sigma_\omega \mu_t)\frac{\partial \omega}{\partial x_j}\right] + \frac{\rho C_\omega}{\mu_t}P_k - \rho \alpha \omega^2$$
$$+ 2(1-f_1)\frac{\rho \sigma_{\omega 2}}{\omega}\frac{\partial k}{\partial x_j}\frac{\partial \omega}{\partial x_j} \qquad (12)$$

The eddy viscosity is obtained from

$$\mu_t = \frac{a_1 \rho k}{\max\left(a_1 \omega, \Omega f_2\right)}, \qquad (13)$$

where the magnitude of vorticity $\Omega = \|curl\ \mathbf{v}\|_2$ and the auxiliary function f_2 is given by;

$$f_2 = \tanh(\arg_2^2)\ , \qquad (14)$$

$$\arg_2 = \max\left[\frac{2\sqrt{k}}{0.09\omega d}, \frac{500\mu}{\rho\omega d^2}\right].$$

The model constants are as follows:

$a_1 = 0.31,\ \alpha^* = 0.09.$ \qquad (15)

The coefficients of the SST model C_ω, α, σ_k and σ_ω are obtained by blending the coefficients of the k-ω model, denoted as ϕ_1, with the coefficients of the k-ε model, denoted as ϕ_2. The corresponding relation is

$$\phi = f_1\phi_1 + (1-f_1)\phi_2\ . \qquad (16)$$

The coefficients of the inner model (k-ω) and of the outer model (k-ε) are given in Equations (17) and (18) respectively,

$\sigma_{k1} = 0.85,\ \sigma_{\omega 1} = 0.500,\ \alpha_1 = 0.0750,\ C_{\omega 1} = 0.533,$ \qquad (17)
$\sigma_{k2} = 1.00,\ \sigma_{\omega 2} = 0.856,\ \alpha_2 = 0.0828,\ C_{\omega 2} = 0.440.$ \qquad (18)

The function f_1 which blends the model coefficients of the k-ω model in boundary layers with the transformed k-ε model in free-shear layers and freestream zones, is defined as

$$f_1 = \tanh(\arg_1^4)\ , \qquad (19)$$

$$\arg_1 = \min\left\{\max\left[\frac{\sqrt{k}}{0.09\omega d}, \frac{500\mu}{\rho\omega d^2}\right], \frac{4\rho\sigma_{\omega 2}k}{CD_{k\omega}d^2}\right\}, \qquad (20)$$

where d is the distance to the closest wall and $CD_{k\omega}$ is the positive portion of the cross-diffusion term in the ω-equation

$$CD_{k\omega} = \max\left[2\rho\sigma_{\omega 2}\frac{1}{\omega}\frac{\partial k}{\partial x_j}\frac{\partial \omega}{\partial x_j}, 10^{-20}\right]. \qquad (21)$$

The boundary conditions for the turbulence kinetic energy and its specific dissipation rate at solid wall are

$$k = 0\ \text{ and }\ \omega = 10\frac{6\mu}{\rho\alpha_1 d_1^2} \qquad (22)$$

where d_1 is the distance of the first node (cell center node) from the wall. The grid has to be refined such that $y^+ < 0.3$.

3. Numerical Method

Computations are performed by an elliptic solver which solves the mean-flow equations and turbulence models using the second-order TVD-upwind scheme based on Van Leer's flux limiter [7]. The transport equations defining the problem are discretized by the finite volume method based on non-staggered grid arrangement, i.e., all variables are stored at the same points. With this approach, the problem domain is divided into a number of small control volumes, the boundaries of control volumes are positioned mid-way between adjacent nodes and thus each node is surrounded by the control volume. The governing equations have been integrated over the control volume to yield the discretized equations at its node. The diffusive and source terms are discretized by using the second-order central differencing scheme and the nonlinear convective term is discretized by using the first-order upwind scheme.

The SIMPLE algorithm is employed to solve all transport equations. The calculation procedure is started with initializing the field variables with a small value except for the pressure that is initialized zero. To initiate the SIMPLE calculation process, the pressure field is guessed and employed to sequentially solve the momentum equation to yield the velocity field. The velocity field is used to determine the mass fluxes through each cell face and subjected to the constraint that it must satisfy the continuity equation. In this step, because of the use of non-staggered grid arrangement, the Rhie-Chow interpolation is used to determine the mass fluxes to take into account for the nonlinear case of the pressure field to avoid the checker-board effect. The pressure-correction equation is performed by using the mass imbalance arising from the incorrect velocity field as the source term so that the pressure-correction field can be obtained at all nodes. Once the pressure-correction field is known, the corrected pressure and velocity fields can be obtained by updating them with the pressure

School of Mechanical Engineering , Suranaree University of Technology

correction. Later, the equations of scalar variables, k and ε, are respectively solved to yield the scalar fields.

During the SIMPLE iteration, the discretized equation is numerically solved by using the relaxation of SIP (Strongly Implicit Procedure) method of Stone (1968). The number of sweeps for each equation solved should not be the same. Only one sweep is sufficient for momentum and turbulent quantities equations but, for the pressure correction, 5-10 sweeps are required. All variables will be weighted with the appropriate values of under-relaxation factor to avoid the solution wiggle. In this work, the value of 0.3 is used to stabilize all variables, except for the pressure correction the value of 0.1 is used.

3.1 Boundary-Fitted Grid Technique

In case of zero pressure gradient boundary layer flow, the computational domain can be selected to be rectangular in shape where the interior grid points are distributed along the grid lines. Therefore, the grid points can be identified easily with reference to the appropriate grid lines. This type of grid is known as the structured grid. Unfortunately, the physical domain of the transitional boundary layer flow in case of non-zero pressure gradient is not rectangular due to the change of the cross sectional area along the flow direction to satisfy the pressure variation in the same direction which is already known in advance from the experimental data. Therefore, imposing a rectangular computational domain on such a physical domain will require some sort of interpolation for the implementation of the boundary conditions. Since the boundary conditions have a dominant influence on the solution of the equation, such an interpolation causes inaccuracies at the places of greatest sensitivity. To overcome these difficulties, a transformation from the physical space (x,y) to the computational space (ξ,η) is adopted here. The transformation is accomplished by specifying a generalized coordinate system which will map the curvilinear grid system in the physical space to a rectangular uniform grid system in the computational space [8]. In the present work, the transformation technique used here is the so-called inverse transformation. With this technique, the transformed governing equation will be expressed in terms of the inverse metrics such as $\partial x/\partial \eta$, $\partial y/\partial \xi$ and the Jacobian J. For all convection-diffusion problems, the transformed governing equation for the property ϕ can be formulated and written in the following general form:

$$\frac{\partial \rho \tilde{u} \phi}{\partial \xi} + \frac{\partial \rho \tilde{v} \phi}{\partial \eta} = \left[\frac{\partial}{\partial \xi}\left(\frac{\alpha_\phi \mu_\phi}{J} \frac{\partial \phi}{\partial \xi} \right) + \frac{\partial}{\partial \eta}\left(\frac{\lambda_\phi \mu_\phi}{J} \frac{\partial \phi}{\partial \eta} \right) \right] \quad (23)$$
$$+ D_\phi + JS_\phi$$

where

$$D_\phi = -\left[\frac{\partial}{\partial \xi}\left(\frac{\beta_\phi \mu_\phi}{J} \frac{\partial \phi}{\partial \eta} \right) + \frac{\partial}{\partial \eta}\left(\frac{\beta_\phi \mu_\phi}{J} \frac{\partial \phi}{\partial \xi} \right) \right]. \quad (24)$$

$$\alpha_\phi = \frac{\partial x}{\partial \eta}\frac{\partial x}{\partial \eta} + \frac{\partial y}{\partial \eta}\frac{\partial y}{\partial \eta} \; , \; \lambda_\phi = \frac{\partial x}{\partial \xi}\frac{\partial x}{\partial \xi} + \frac{\partial y}{\partial \xi}\frac{\partial y}{\partial \xi} \; ,$$

$$\beta_\phi = \frac{\partial x}{\partial \xi}\frac{\partial x}{\partial \eta} + \frac{\partial y}{\partial \xi}\frac{\partial y}{\partial \eta} \; , \quad (25)$$

$$\tilde{u} = u\frac{\partial y}{\partial \eta} - v\frac{\partial x}{\partial \eta} \; , \; \tilde{v} = -u\frac{\partial y}{\partial \xi} + v\frac{\partial x}{\partial \xi} \; . \quad (26)$$

In the present study, the SIMPLE algorithm is employed to solve all transport equations as already mentions above. Since this algorithm deals with the continuity via the pressure correction formula which is expressed in form of the central difference formulation of the Poisson equation, not in the general form of the convection-diffusion transport equation as in the momentum and turbulence transport equations. Hence, to transform the pressure-correction equation from the physical space to the computational space, a new derivation of such an equation has been deliberately performed. Eventually, the general form of the pressure correction equation can be written in the following form:

$$a_P p'_P - a_W p'_W - a_E p'_E - a_N p'_N - a_S p'_S = B_m \quad (27)$$

with the coefficients and source terms are given below:

$$a_W = \rho(\Delta\eta)^2 B_{u,w} \; , \; a_E = \rho(\Delta\eta)^2 B_{u,e} \; ,$$
$$a_S = \rho(\Delta\xi)^2 C_{v,s} \; , \; a_N = \rho(\Delta\xi)^2 C_{v,n} \; , \quad (28)$$
$$B_m = (\rho\tilde{u}\Delta\eta)_w - (\rho\tilde{u}\Delta\eta)_e + (\rho\tilde{v}\Delta\xi)_s - (\rho\tilde{v}\Delta\xi)_n \; ,$$

where

$$B_u = \frac{1}{J}\left[\frac{1}{a_P^u}\frac{\partial y}{\partial \eta}\frac{\partial y}{\partial \eta} + \frac{1}{a_P^v}\frac{\partial x}{\partial \eta}\frac{\partial x}{\partial \eta} \right] , \quad (29\text{-}1)$$

$$C_v = \frac{1}{J}\left(\frac{1}{a_P^u}\frac{\partial y}{\partial \xi}\frac{\partial y}{\partial \xi} + \frac{1}{a_P^v}\frac{\partial x}{\partial \xi}\frac{\partial x}{\partial \xi} \right) . \quad (29\text{-}2)$$

and the Jacobian J is denoted by

$$J = \begin{vmatrix} \dfrac{dx}{d\xi} & \dfrac{dy}{d\xi} \\ \dfrac{dx}{d\eta} & \dfrac{dy}{d\eta} \end{vmatrix} \quad (30)$$

Actually, the transformation of flow problems from the physical space to computational space always results in the complexity of the governing equation form. However, the advantage of this method is that the grid points greatly fall on the curvature surfaces of the domain boundaries which are convenient in specifying the boundary condition.

3.2 Description of Test Cases

Test cases presented in this paper are the ERCOFTAC T3-series of flat plate experiments. All test cases are

School of Mechanical Engineering , Suranaree University of Technology

commonly used as benchmarks for the transition prediction by turbulence models. All test cases (T3C1, T3C2 and T3C4) have the non-zero pressure gradient with the freestream turbulence intensity of 7.5%, 3.0% and 3.0% respectively corresponding to the transition in bypass mode. T3C1 and T3C2 cases are the test cases specially designed to test the ability of turbulence models in predicting the transition with the continuous variation of pressure gradients representing an aft-loaded turbine blade [1]. The T3C4 test case consists of a flat plate with favorable and adverse pressure gradient imposed by the opposite converging/diverging wall. It is usually used to test the model ability to predict the separation induced transition [3]. Domain of computation used here is the flat plate of 1.5 m long, and the Reynolds numbers based on the plate length, Re_L, are 5.9×10^5, 5.4×10^5 and 1.2×10^5 for T3C1, T3C2 and T3C4 cases, respectively. The thickness of the domain at the entrance region before the leading edge is 0.22 m. and then varies along the streamwise direction corresponding to the pressure gradient variation afterward.

The computational domain begins at 0.15 m. upstream of the plate leading edge to facilitate an unambiguous specification of freestream conditions. This is vital because it enables the uniform profiles of k and ω to be assigned. If one starts computations at the plate leading edge, the predicted transition point is strongly dependent on the assumptions made for the way k and ω vary across the boundary layer [9]. In computations, a variety of grid densities is explored by performing a grid-independent check, in which the grid spacing is decreased by half in both directions, and a mesh of 155 (streamwise) × 100 (expanding from wall to freestream) H-type grid is adopted for all test cases. In all cases, the first node adjacent to the wall is located at y^+ below 0.3.

In this study, incompressible flow is considered so that the fluid density and molecular viscosity are constant which are 1.2 kg/m^3 and 1.8×10^{-5} kg/m·s respectively. The SIMPLE algorithm is employed to solve all transport equations. The initial streamwise mean velocity profile is the Blasius velocity profile, and the inlet conditions are prescribed to reproduce the experimental decay of the freestream turbulence intensity. The isotropic turbulence is assumed, so that the inlet turbulence kinetic energy is obtained from the experimental inlet freestream turbulence intensity, Tu_{in}, and the inlet viscosity ratio, $R_\mu = \mu_t/\mu$, is specified in order to mimic the experimentally measured decay of the freestream turbulence intensity. Hence, the inlet conditions of the turbulent variables are calculated from the following relationships:

$$\mu_t = R_\mu \mu \,, \ k = (3/2)(Tu_{in} \cdot U_{in})^2 \,, \ \omega = \rho k / \mu_t \,,$$
$$\tilde{\varepsilon} = \rho C_\mu k^2 / \mu_t \,, \tag{31}$$

where Tu_{in} denotes the inlet freestream turbulence intensity (%), and U_{in} is the inlet velocity. For the outlet boundary, all variables are extrapolated from nodes inside the domain to the outer boundaries. Details of inlet

conditions of all test cases are given in Table 1, and the inlet conditions of turbulent variables are obtained by matching the decay of freestream turbulence intensity with the experimental data show in Fig. 1.

Table 1. Summary of inlet conditions of all test case

Case	U_{in} (m/s)	Tu_{in} (%)	μ_t/μ
T3C1	5.9	7.5	44.0
T3C2	5.0	3.0	7.0
T3C4	1.2	3.0	2.0

Generally, the appropriate value for the inlet viscosity ratio matching with the experimental decay of the freestream turbulence intensity is not too much difficult to observe, and normally such a value can be found in less than four times by numerical experiments. The more difficult task than the previous step is to observe the appropriate domain shape to match the experimental data of the pressure gradient variation of each test case. The possible way to find that shape, which is used in the present work, is to compute the mass flux through each cross section of the domain using the velocity values at freestream which is known from the experimental data. Using the concept of mass balance, the thicknesses of the cross sections along the flow direction can simply be computed and are shown in Figs. 2-4 (a).

4. Results and Discussion

The predicted results of two turbulence models are compared with the experimental data of the momentum thickness Reynolds number, Re_θ, the skin friction coefficient, C_f, and the shape factor, H. (i) The momentum thickness Reynolds number is directly related to the momentum thickness of the boundary layer which indicates the development of the boundary layer. In case of the boundary layer flow on a flat plate, the boundary layer is laminar in the entrance region of the flat plate, and becomes transitional and then turbulent. According to Thwaites' method [10], the momentum thicknesses of laminar boundary layers can be determined from $\theta = 0.671x/Re^{1/2}$, displayed by the dash lines in Fig. 2-4 (b). For the profile of the momentum thickness Reynolds number along the flat plate, the transition starts at the point where the profile deviates from the laminar line, and ends at the point where the profile touches the turbulence line. (ii) The skin friction coefficient is an important factor for indicating the starting and ending points of transition, and also indicates the growth rate characteristic of transition leading to the length of transition to be found. The variation of the skin friction coefficient along the flat plate is usually displayed with respect to the Reynolds number, and the linear-scale plot is displayed in this work. The start and end of transition occur at the points where the skin friction coefficient profile deviates from the laminar value and approaches to the turbulent value respectively, and the variation between these two points indicates the growth rate and length of transition (the more the rapid growth rate; the shorter the transition length). (iii) The shape factor defined as the ratio of the displacement thickness to the

School of Mechanical Engineering , Suranaree University of Technology

momentum thickness in the boundary layer ($H=\delta^*/\theta$) describes the influence of the freestream turbulent eddies on transition. Moreover, it indicates if the boundary layer is separated or has the tendency to separate. Moreover, the shape factor also indicates the region where the boundary layer tends to be turbulent. A decrease in the shape factor implies that the transition to turbulent boundary layer is about to occur.

For T3C1 case, the flow is subjected to the freestream turbulence intensity of 7.5% at the inlet, and the comparison of the predicted results with the experimental data is shown in Fig. 2. The SST model gives no flow transition and remains fully turbulent flow for the entire flow regime. This model gives the immediate transition to turbulence at the leading edge of the flat plate showing almost no laminar zone. This is because the predicted profile of momentum thickness Reynolds number deviates from the experimental one at the leading edge location. As a result, the skin friction coefficient predicted by this model follows the turbulent skin friction coefficient, and the immediate decay of the shape factor at the leading edge is found. With the Launder and Sharma model, the model gives good predicted results for the boundary layer development and then reproduces the shape factor profile fairly well but gives too early changes in the skin friction coefficient.

For T3C2 case, the flow is subjected to the freestream turbulence intensity of 3.0% at the inlet and the comparison of the predicted results with the experimental data is shown in Fig. 3. As in the previous case, the SST model shows the flow transition at leading edge without displaying any laminar behaviour. With the Launder and Sharma model, the model reproduces the developing layer fairly well but gives too early changes in the skin friction coefficient and shape factor.

For T3C4 case, the flow is subjected to the freestream turbulence intensity of 3.0% at the inlet and the comparison of the predicted results with the experimental data is shown in Fig. 4. The SST model again gives the same conclusion as in the previous two cases, that is, it cannot detect any effect of transition, and therefore gives an immediate transition to turbulence at the leading edge of the flat plate. With the Launder and Sharma model, the model shows a good result for almost all upstream regions, but, for downstream region near the exit of the flat plate, the predicted results deviate from the experimental data. This downstream region is affected by the adverse pressure gradient leading to the reverse flow and such flow usually fails to be predicted by this model.

5. Conclusion

The method of converting the effect of the pressure gradient variation to the domain thickness variation has been investigated in the transitional boundary layer with non-zero pressure gradient. The method solves the full equations of fluid motion using the boundary-fitted grid transformation technique. Two turbulence models: the SST model of Menter [5] and the k-ε model of Launder and Sharma [4], are implemented and their abilities are assessed. The SST model gives fully turbulent results for

all cases and cannot detect any transition effect. The Launder and Sharma model gives good results for T3C1 and T3C2 cases but predicts the transition onset too early and the transition length too short. For T3C4 case, the Launder and Sharma model can predict the reverse flow behaviour which appears near the end region of the flat plate but cannot detect the transition behaviour accurately in such region.

References

[1] Suzen, Y.B., Huang, P.G., 2001. Predictions of separated and transitional boundary layers under low pressure turbine airfoil conditions using an intermittency transport equation. AIAA 200-0446, 39th AIAA Aerospace Sciences Meeting & Exhibit, Reno, Nevada, January 8-11.

[2] Chen, W.L., Lien, F.S., and Leschziner, M.A., 1998. Non-linear eddy-viscosity modeling of transition boundary layers pertinent to turbomachine aerodynamics. J. Heat and Fluid Flow 19, pp. 297-306.

[3] Langtry, R.B., and Menter, F.R., 2005. Transition modeling for general CFD applications in aeronautics. AIAA 2005-522.

[4] Launder, B.E., and Sharma, B., 1974. Application of the energy dissipation model of turbulence to the calculation of flow near a spinning disk. Letters in Heat and Mass Transfer 1, pp. 131-138.

[5] Menter, F.R., 1994. Two-equation eddy-viscosity turbulence models for engineering applications. AIAA 32, pp. 1598-1605.

[6] Coupland, J., 1993. ERCOFTAC Classic Database. http://cfd.me.umist.ac.uk/ercoftac/ (accessed on May 2005.

[7] Van Leer, B., 1977. Towards the ultimate conservative difference scheme. iv. a new approach to numerical convection. J. Comput. Phys. 23, pp. 276-299.

[8] Hoffmann, K.A., and Chiang, S.T., 1995. Computational fluid dynamics for engineers. 3rd Edition, Vol. 1.

[9] Craft, T.J., Launder, B.E., Suga, K., 1997. Prediction of turbulence transition phenomena with a nonlinear eddy-viscosity model. J. Heat and Fluid Flow 18, pp.15-28.

[10] Thwaites, B., 1949. Approximate calculation of the laminar boundary layer. Aeronaut. Q., Vol. 1, pp. 245-280.

School of Mechanical Engineering , Suranaree University of Technology
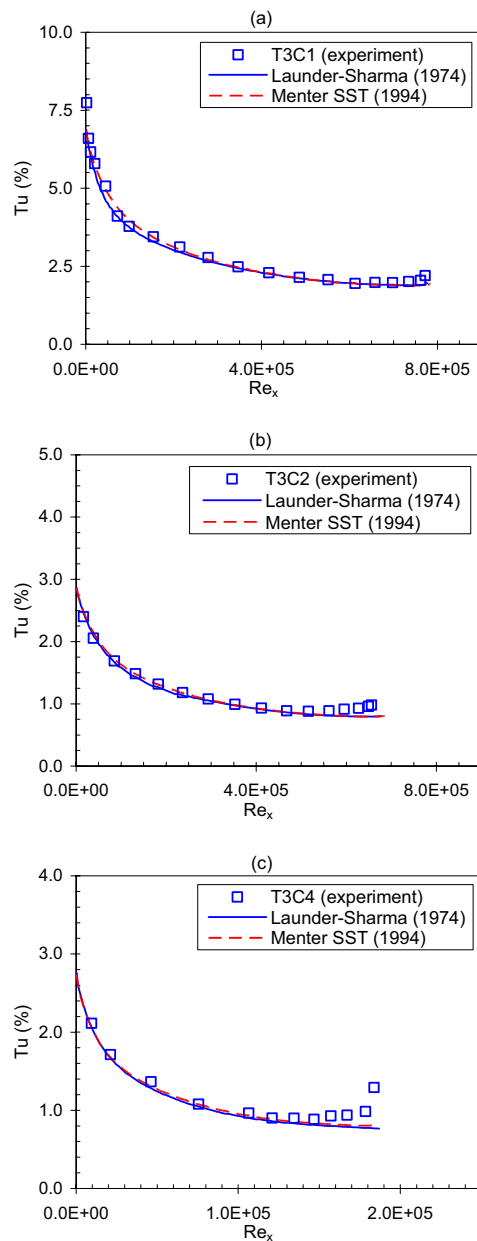
Fig. 1. Comparison of the measured freestream turbulence intensities with the numerical results for (a) T3C1, (b) T3C2, and (c) T3C4 cases.
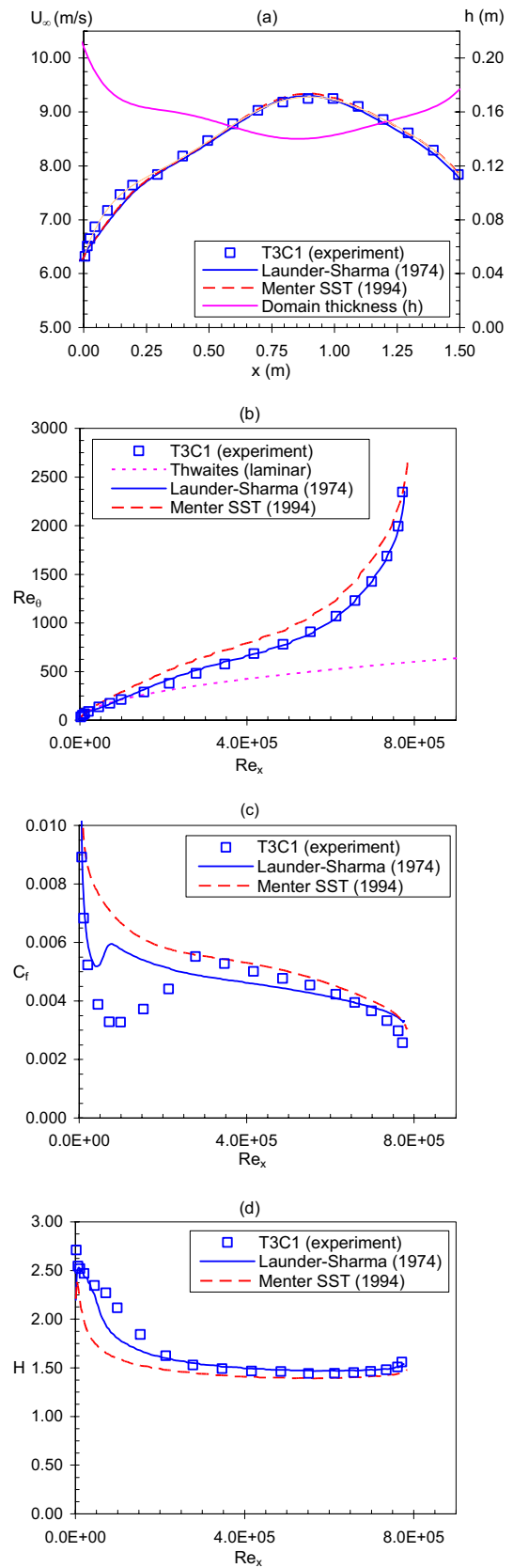
Fig. 2. (a) Freestream velocity and domain thickness, (b) Momentum thickness Reynolds number, (c) Skin friction coefficient, and (d) Shape factor for T3C1 case.

School of Mechanical Engineering , Suranaree University of Technology
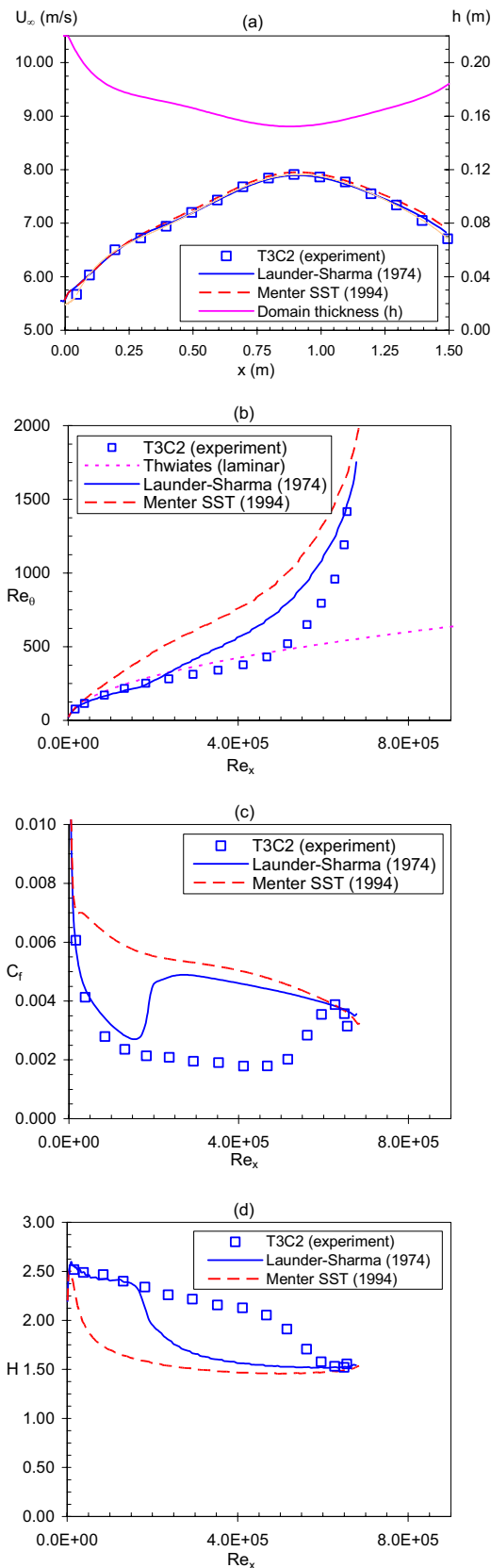
Fig. 3. (a) Freestream velocity and domain thickness, (b) Momentum thickness Reynolds number, (c) Skin friction coefficient, and (d) Shape factor for T3C2 case.

Fig. 4. (a) Freestream velocity and domain thickness, (b) Momentum thickness Reynolds number, (c) Skin friction coefficient, and (d) Shape factor for T3C4 case.

School of Mechanical Engineering , Suranaree University of Technology